






Article

New Insight into the Microstructure Changes and Molecular Mobility of Polyamides Exposed to H₂S Scavengers

Marina Perassoli de Lazari ¹, Antonio Henrique Monteiro da Fonseca Thomé da Silva ^{2,3},
Rodrigo Henrique dos Santos Garcia ¹, Sylvia Correa dos Santos Teixeira ², João Eduardo de Oliveira ¹,
Érica Gervasoni Chaves ², Luiz Antônio de Oliveira Nunes ¹, Hercílio de Angeli Honorato ²,
Sonia Maria Cabral de Menezes ⁴, Aline Pinde Lima ², Luiz Silvino Chinelatto Junior ²,
and Eduardo Ribeiro de Azevedo ^{1,*}

¹ Instituto de Física de São Carlos, Universidade de São Paulo, 400 Parque Arnold Schmidt, São Carlos 13566-590, SP, Brazil

² PETROBRAS/CENPES, Av. Horácio Macedo 950, Rio de Janeiro 21941-915, RJ, Brazil; hercilio.deangeli@petrobras.com.br (H.d.A.H.); alineplima@petrobras.com.br (A.P.L.); lsilvino@petrobras.com.br (L.S.C.J.)

³ Departamento de Engenharia Mecânica, Universidade Federal Fluminense—UFF/PGMEC, Niterói 24210-240, RJ, Brazil

⁴ Instituto de Física, Universidade de São Paulo, Rua do Matão 1371, Cidade Universitária, São Paulo 05508-090, SP, Brazil; scdemenezes@yahoo.com

* Correspondence: azevedo@ifsc.usp.br

Abstract: Polyamides (PAs) are widely used as barrier materials in offshore oil and gas (O&G) equipment due to their mechanical strength and chemical resistance. However, long-term exposure to hydrogen sulfide scavengers (H₂S-SCVs) may significantly affect their physicochemical properties. Previous studies using thermal analysis and ¹H time-domain NMR (¹H TD-NMR) suggest that ethoxylated H₂S-SCVs impose molecular constraints, increasing the glass transition temperature (T_g) and reducing chain mobility above T_g. The present study builds upon these findings using a multi-technique analytical approach, including FTIR, Raman, ¹H DQ-TD-NMR, and ¹³C solid-state NMR (ssNMR), to provide a more comprehensive understanding of the molecular alterations in PA materials. The results clearly demonstrate that H₂S-SCV exposure leads to the progressive exudation of plasticizers from the PA matrix. This plasticizer loss is a key factor contributing to the observed shift in T_g and the reduction in molecular mobility. ¹H DQ-TD-NMR data confirmed an increase in the density of dynamically constrained chains over time and allowed for the characterization of heterogeneity in these constraints throughout the PA matrix. Moreover, ¹³C ssNMR spectra revealed the presence of immobilized H₂S-SCV chemical groups within the polymer matrix, strongly supporting the early statement that the mobility constraints observed in ¹H DQ-TD-NMR are associated with the formation of crosslinks induced by the H₂S-SCV: H₂S-SCV acts as a crosslinking agent. Taken together, our findings indicate that both plasticizer loss and H₂S-SCV-induced crosslinking contribute significantly to the microstructural evolution of PAs when exposed to ethoxylated H₂S-SCVs, offering important insights into their degradation mechanisms and long-term behavior in aggressive operational environments.

Keywords: ¹H time-domain NMR; solid state ¹³C NMR; infrared spectroscopy; polyamide degradation; H₂S scavenger; plasticizer exudation



Academic Editor: Takayasu Kawasaki

Received: 26 April 2025

Revised: 4 June 2025

Accepted: 6 June 2025

Published: 12 June 2025

Citation: Lazari, M.P.d.; Silva, A.H.M.d.F.T.d.; Garcia, R.H.d.S.; Teixeira, S.C.d.S.; Oliveira, J.E.d.; Chaves, É.G.; Nunes, L.A.d.O.; Honorato, H.d.A.; Menezes, S.M.C.d.; Lima, A.P.; et al. New Insight into the Microstructure Changes and Molecular Mobility of Polyamides Exposed to H₂S Scavengers. *Polymers* **2025**, *17*, 1634. <https://doi.org/10.3390/polym17121634>

Copyright: © 2025 by the authors. Licensee MDPI, Basel, Switzerland. This article is an open access article distributed under the terms and conditions of the Creative Commons Attribution (CC BY) license (<https://creativecommons.org/licenses/by/4.0/>).

1. Introduction

Polymers are key materials in numerous contemporary technological applications. For instance, active polymer layers constitute the core of various organic electronic semiconductor devices, including polymer-based Light-Emitting Diodes (LEDs), transistors, flexible solar cells, and neuromorphic memories [1,2]. Despite the widespread use of active polymers in advanced applications, their significant utility remains closely tied to conventional polymers. These polymers find applications in textiles, construction, plastics, rubber, oil and gas, and various other industrial sectors.

Even in more traditional polymer applications, significant technological advancements have been made in materials production. These advancements have led to remarkable improvements in mechanical strength, durability, flexibility, permeability to liquids and gases, and resistance to degradation, among other properties. It is worth noting that each improvement is tailored to the specific application and type of polymer, with enhanced resistance to degradation being a common focus across diverse applications.

In a broad context, polymer degradation is linked to the interaction of polymer chains with external agents, resulting in changes to the chemical composition, microstructure, morphology, or dynamics of the polymer chains, thereby affecting desired macroscopic properties. Consequently, comprehending the degradation mechanism and its connection with the macroscopic properties of interest is essential for developing strategies that either mitigate polymer degradation or prevent conditions that promote the degradation process.

Polymeric materials play a widespread role in the oil and gas (O&G) industry, particularly within the infrastructure used in offshore production [3]. In these applications, one of their primary functions is in the design of flexible pipelines, where polymer layers not only serve as a fluid barrier for the metal layers but also provide crucial design protection against corrosion and abrasion of the subsequent metal components in the structure. Consequently, the premature failure of the polymeric barrier layer during pipeline service can result in substantial costs and pose potential environmental hazards, emphasizing the critical need for its integrity in the flexible pipeline design process [3–6].

Apart from mechanical integrity, maintaining the characteristics of the polymer layers, particularly their performance related to gas and liquid permeation, is equally important. This is significant due to the presence of typical fluids such as oil, water, H_2S , CH_4 , or CO_2 , which may commonly be encountered in offshore production [6].

Among the construction polymers utilized in the oil and gas (O&G) industries, polyamide (PA, $[(CH_2)_xCONH]_n$) stand out as a semi-crystalline thermoplastic extensively employed in various applications. It is commonly used in external anticorrosion coatings for flexible pipes, umbilicals and their accessories, valves, and even as a coating for parts with complex geometries designed for different operating conditions [6]. PA exhibits unique physical properties and good chemical resistance, serving as an effective barrier material during the transportation of gas, water, and oil mixtures for specific scenarios, given that oxidation and/or hydrolysis degradation processes are duly controlled [6].

Hydrolysis is recognized as the primary degradation pathway in humid and acidic environments, where water molecules catalyze the cleavage of amide (C–N) bonds along the polymer backbone. This process results in a reduction of the polymer's molecular weight and, consequently, in a deterioration of mechanical properties such as tensile strength and elongation at break. Monitoring molecular weight is thus essential in assessing the service life of PA-based systems. The most common method used for this purpose is the determination of the inherent viscosity (IV) in sulfuric acid, which correlates with average molecular weight. The industry-standard API 17 TR2 guideline relies on CIV (corrected inherent viscosity) values to classify material suitability and define safe operational envelopes based on long-term laboratory aging and mechanical test results.

Beyond hydrolysis, interactions of PA with chemicals used in offshore production and transportation can also induce the degradation of the polymer. This is particularly relevant in scenarios where subsea injection of chemicals, including H₂S-SCVs, is crucial. Consequently, when assessing the service life of PA pressure sheaths, global oil producers and flexible pipe manufacturers commonly monitor corrected inherent viscosity (CIV), following the API 17 TR2 methodology.

However, CIV-based assessments focus solely on molecular weight and may overlook other degradation mechanisms that do not involve significant chain scission. For example, chain crosslinking, microstructural rearrangements, or increased dynamic constraints in the amorphous phase can compromise material performance without necessarily reducing molecular weight. These limitations highlight the need for complementary diagnostic methods capable of detecting subtler or alternative degradation effects.

While there is a reasonable number of works employing spectroscopic techniques to elucidate the structure of H₂S-SCV [7–9], only a few delve into changes in the microstructure and chain dynamics of the polymers exposed to these fluids [5,10]. Among them is our previous study, where ¹H time-domain nuclear magnetic resonance (¹H TD-NMR) methods were applied to investigate the effects of H₂S-SCV exposure on the microstructure and dynamics of PA chains [10]. TD-NMR is a non-destructive, sensitive, and relatively low-cost technique that probes molecular mobility and segmental dynamics, thus offering insights into microstructural and morphological changes at the molecular level. These studies indicated that exposure to H₂S-SCVs introduces mobility constraints on PA chains within the amorphous phase, shifting the onset of molecular motions associated with the glass transition to higher temperatures. Furthermore, ¹H DQ-TDNMR experiments in the polymer's melt state revealed an increase in the density of constrained points in the polymer chains and a decrease in the amount of highly mobile segments upon exposure to H₂S-SCVs. A specific analysis of the data considering a power law correlation function for the segmental dynamics [11] suggests a scenario with the prevalence of fixed constraining points, as is consistent with the crosslinking of PA chains due to interactions with H₂S-SCVs. Furthermore, these results were not only correlated to more macroscopic changes observed in CIV and differential scanning calorimetry (DSC) measurements but were also capable of detecting microstructural and dynamical alterations not captured by CIV or DSC measurements.

Despite these findings, several crucial aspects remain unclear, including the effect of exposure temperature, the type of H₂S-SCV, the mixture of H₂S-SCVs with other production fluids used in O&G production, and, importantly, a more specific molecular characterization and its relationship with the change observed in the microstructure and chain mobility.

In this article, we conducted a comprehensive characterization of the long-term exposure of commercial PA to H₂S-SCVs (up to 60 days at 40 °C), with a primary focus on the molecular origin of the microstructure changes. To achieve this, infrared and Raman optical spectroscopy, ¹³C solid-state NMR, and ¹H time-domain nuclear magnetic resonance (¹H TD-NMR) were employed and jointly analyzed. In addition, the samples were prepared with a batch of commercial PA and an ethoxylated H₂S-SCV different from that used in Reference [10].

The ¹³C solid-state NMR, Raman and FTIR spectroscopic results demonstrate that long-term contact with these scavengers leads to the exudation of plasticizers from the PA matrix. This phenomenon explains the observed shift to higher temperatures in the onset of molecular motions related to the glass transition in samples exposed to H₂S scavengers, as revealed by ¹H TD-NMR. The new analysis of the ¹H DQ-TDNMR results confirmed the progressive PA increase in the density of dynamically constrained chains (previously suggested as crosslinking points in [10]) with the exposure to the H₂S-SCV. Furthermore,

the ^1H DQ-TDNMR experiments in the new set of the samples were designed to allow for a distinct analysis, providing information on the heterogeneity of the dynamic constraints along the samples. A clear trend of increasing heterogeneity over time of exposure was observed. Additionally, the presence of chemical groups of the H_2S scavenger immobilized in the polymer matrix was found by ^{13}C solid-state NMR, thus supporting the idea that the fixed dynamic constraints observed by ^1H DQ-TDNMR are associated with PA chain crosslinks, and it also suggests that the H_2S -SCVs play a role in the crosslinking process. These findings suggest that both the formation of crosslinks and the loss of plasticizers contribute to the observed rise in glass transition temperature and the reduction in chain mobility in the molten state, consistent with the formation of a new crystalline phase, as observed in the DSC results of [10] and the gelation of the samples in meta-cresol, which impeded the VIC measurement in samples exposed to H_2S -SCVs. Furthermore, because the TD-NMR results depicted the same behavior as reported in Reference [10], even though a different H_2S -SCV and new batch of PA samples were used, it is possible to suggest that this behavior can be generalized to other types of ethoxylated scavengers.

2. Materials and Methods

Samples: Typical flexible pipe-grade PA was used. The PA samples were cut into cylindrical pieces, with a 4 mm diameter, for ^{13}C solid-state NMR and ^1H TD-NMR measurements. Samples of non-exposed PA and PA exposed to pure H_2S -SCV for 5, 15, 45, and 60 days at 40°C were studied. The identification of samples was presented as PA-# days, where # is the number of exposure days. The maximum exposure time of 60 days was chosen based on preliminary observations indicating that very little additional change occurred beyond 60 days. The exposure temperature of 40°C was chosen to minimize the risk of hydrolysis, which is known to occur in polyamides at temperatures above 60°C , even in the presence of trace amounts of water [12–14]. To avoid the overlapping of these distinct degradation processes, we chose to perform the exposure at 40°C , where hydrolysis is significantly less likely to occur. This allowed us to isolate the effects of the H_2S scavenger on the microstructure of PA11. Attempts to determine the corrected inherent viscosity (CIV) were made for all samples, following the API 17 TR2 methodology, using the same procedure as described in Reference [10]. In this procedure, before the inherent viscosity determination, samples must be solubilized in meta-cresol at 100°C for 1 h. However, samples that were in contact with pure H_2S -SCV from this study did not solubilize in this solvent under standard conditions, and thus their CIV could not be measured. Thus, it was only possible to measure the CIV for the PA sample not exposed to the H_2S ; its CIV was found to be 1.6 ± 0.1 dL/g.

NMR experiments: Low-field ^1H TD-NMR experiments were performed in a 0.5 T Bruker Minispec mq20 NMR analyzer (^1H frequency of 20 MHz), using a VT probe head with dead time of $12.5\ \mu\text{s}$. $\pi/2$ and π pulse lengths of 2.5 and $4.8\ \mu\text{s}$, respectively, and recycle delays of 2 s were used. Dipolar-filtered MSE (DF-MSE) pulse sequence (see Figure 1 and References [10,15,16]) were performed with MSE echo times of $100\ \mu\text{s}$ and a dipolar filter time of $40\ \mu\text{s}$. The variable temperature DF-MSE measurements were performed in a multi-step form, using 10°C temperature steps and a stabilization period of 10 min. Temperature variation comprised an ascendant range from 20°C to 200°C , followed by a descendant range from 200°C to 20°C . ^1H DQ-TDNMR experiments were carried out using double-quantum evolution times, ranging from 0.2 to 10 ms. The data was acquired using the pulse sequence and phase cycling described in Reference [17]. A total of 128 scans were acquired in all experiments. ^1H DQ-TDNMR measurements were performed at 200°C , which is above the melting temperature of PA. To guarantee that the samples were in the melt state during the ^1H DQ-TDNMR measurements, mixed-MSE was performed at 200°C , showing

no sign of rigid components in the samples. ^1H DQ-TDNMR is being extensively used for probing the presence of crosslinks and entanglements in polymer networks, being an alternative to solvent-base swelling techniques, with many comparisons between crosslink density measure by swelling and ^1H DQ-TDNMR available in the literature [17–19].

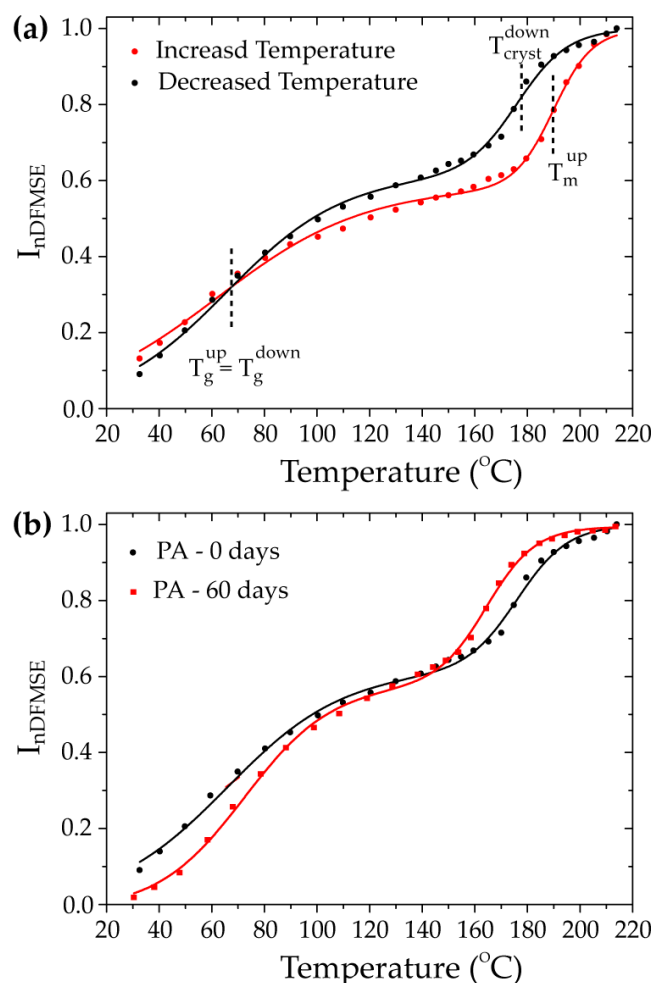


Figure 1. $I_{nDFMSE}(T)$ vs. T curves measured for several PA samples. (a) Comparison between $I_{nDFMSE}(T)$ vs. T curves of non-exposed PA samples acquired at increasing and decreasing temperatures. (b) Comparison between $I_{nDFMSE}(T)$ vs. T curves of PA samples not exposed to the H₂S-SCV for 60 days at 40 °C, acquired at decreasing temperatures.

Fourier-Transform Infrared Spectroscopy (FTIR): FTIR absorbance experiments were conducted using a Magna-IR 850 Series II-Nicolet Spectrometer in the wavelength range of 4000 cm^{-1} to 15,000 cm^{-1} , with a resolution of 8 cm^{-1} , on samples with a standardized thickness of approximately 1 mm. The surfaces of the samples were prepared and uniformed using successive abrasions with 400–1200-grit sandpaper. A quartz beam splitter and a tungsten light bulb were used, along with an InGaAs detector.

Raman spectroscopy: Raman spectroscopy experiments were conducted using Ocean Optics QE66 Pro equipment within a wavelength ranging from 200 cm^{-1} to 1800 cm^{-1} . Ten scans per experiment were performed using a 780 nm laser with a power output of 1000 mW.

3. Results

3.1. Effects of the H₂S-SCVs on the Microstructure and Dynamics of PA

To obtain information about overall changes in the PA chain mobility induced by the exposure to the H₂S-SCVs, we employed a ¹H TD-NMR experiment known as DF-MSE, which combines the Goldman–Shen dipolar filter (DF) and mixed-MSE. Details of this experiment are described in References [10,16], and its application to probe mobility transitions in PA is explained in Reference [10].

In general terms, this experiment yields a normalized signal intensity, I_{nDFMSE} , which accounts exclusively for mobile molecular segments—segments that undergo motion with rates higher than that of the 1H-1H magnetic dipolar coupling, typically in the order of 50 kHz. Therefore, by monitoring the I_{nDFMSE} as a function of temperature, it becomes possible to directly detect the onset temperature of molecular mobility processes through the increase in I_{nDFMSE} . This is illustrated in Figure 1a, which shows I_{nDFMSE} vs. T for PA not exposed to the H₂S-SCV (PA—0 days).

As observed, there are two main intensity upturns on the I_{nDFMSE} intensity as a function of temperature, associated with the glass transition and the melting of the PA chains. Note, however, that the time scale of the motions detected as mobility is about three orders of magnitude faster than those associated with typical DSC transitions. Consequently, the DF-MSE transition temperature is typically 40 °C higher than the typical temperature expected by DSC for the same process [20].

Typically, each intensity upturn, i , in the I_{nDFMSE} vs. T can be well represented by a sigmodal curve, with the temperature at the inflection point denoted by $T_i^{1/2}$, and the half-width of the transition region given by σ_i . Thus, $T_i^{1/2}$ can be considered the average transition temperature, and σ_i is somewhat related to the heterogeneity of the transition. Under these assumptions, one can fit the I_{nDFMSE} vs. T curve for PA, shown in Figure 1, assuming a sum of two sigmodal curves weighted by a fraction, f_i , to obtain the glass transition and melting temperatures, as well as the corresponding widths and the weights, as seen in the DF-MSE experiment. The values of the parameters $T_i^{1/2}$, σ_i , and f_i obtained from this fitting are shown in Table 1, where $i = 1$ refers to the mobility transition associated with the glass transition, and $i = 2$ refers to the transition associated with the melting of the sample.

Table 1. Parameters extracted from DF-MSE vs. temperature.

| Sample | $T_1^{1/2}$ (°C) | $T_2^{1/2}$ (°C) | σ_1 (°C) | σ_2 (°C) | f_1 | f_2 |
|------------|------------------|------------------|-----------------|-----------------|-------------|-------------|
| PA—0 days | 66 ± 2 | 176 ± 1 | 22 ± 1 | 10 ± 1 | 0.62 ± 0.01 | 0.38 ± 0.01 |
| PA—60 days | 74 ± 1 | 165 ± 1 | 17 ± 1 | 9 ± 1 | 0.59 ± 0.01 | 0.41 ± 0.01 |

As depicted in Figure 1a and summarized in Table 1, the I_{nDFMSE} vs. T curves exhibit differences when acquired with increasing or decreasing temperatures. Notably, the primary distinction lies in the temperature of the high-temperature transition, which is associated with the melting (increasing temperature) and crystallization (decreasing temperature) of PA. This is an expected behavior which happens due to the erasure of the thermal history of the polymer and because the crystallization temperature and fraction (degree of crystallinity) are dependent on the temperature-decrease rate. In addition, as anticipated, the transition temperature associated with the glass transition is about the same for the curves obtained at increasing and decreasing temperatures. The only observed difference is a less spread transition temperature, indicative of more homogeneous dynamics across the sample.

Taking into account the preceding discussion, to detect the effect of the exposure to H₂S-SCV, we conducted DF-MSE measurements at descending temperatures. Specifically, we initiated the measurements from the molten state of PA, progressively decreasing the temperature at 10 °C/min, with stops of 10 min for temperature equilibration and 10 min for measurement at constant temperature. By starting from the melt state and performing the same temperature-decreasing rate and measurement routine, the I_{nDFMSE} vs. T curves should only reflect permanent changes in the mobility transitions induced by the H₂S-SCV.

Figure 2b shows a comparison between the I_{nDFMSE} vs. T curves of the PA not exposed and exposed to the H₂S-SCV at 40 °C for 60 days (PA—60 days). As can be observed in Figure 1 and Table 1, the sample exposed to the H₂S-SCV clearly shows an increase in the transition temperature associated with the glass transition, indicating a higher mobility restriction during this process. This is the same behavior observed in Reference [10], but here we used a new batch of PA, a different ethoxylated H₂S-SCV, and the curves here acquired for pre-molten samples. Thus, the increase in the lower temperature transition on the I_{nDFMSE} vs. T curves confirms that the exposure to ethoxylated H₂S-SCV induces a permanent modification in the mobility behavior during the glass transition of the PA chains.

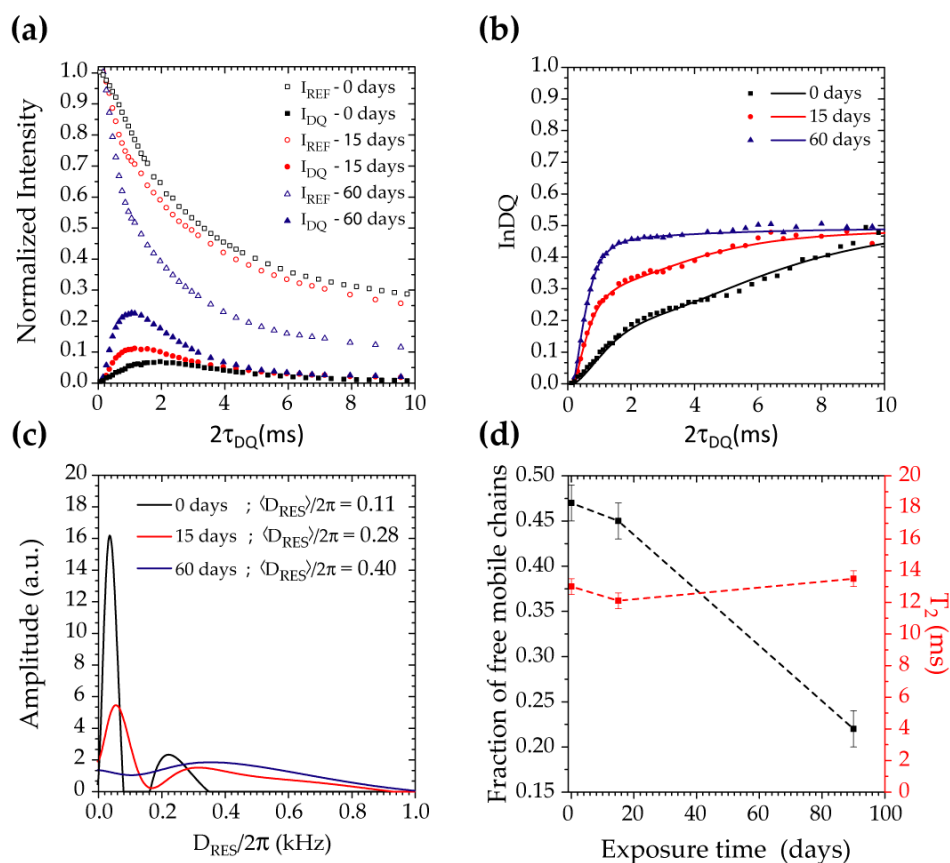


Figure 2. (a) $I_{REF}(\tau_{DQ})$ vs. τ_{DQ} and $I_{DQ}(\tau_{DQ})$ vs. τ_{DQ} curve measured with Baum and Pines pulse sequence [17,21] for PA exposed to H₂S-SCV for several days. (b) $I_{nDQ}(\tau_{DQ})$ vs. τ_{DQ} curve obtained from the data shown in (a), using the procedure described in the text and Equation (1). (c) Distribution of residual dipolar coupling, D_{RES} , obtained from the FITREG program described in References [18,19]. (d) Fraction of free mobile chains and corresponding T_2 values obtained from the data shown in (a), using the procedure described in the text.

¹H DQ-TDNMR experiments were performed using the Baum and Pines pulse sequence described in Reference [21]. The first aim of these experiments was to confirm in this set of samples our previous finding that exposure to the H₂S-SCV induces permanent

mobility restrictions that could be detected in the melt state of the samples [10]. Thus, to guarantee that all samples would be melted and have similar overall mobilities, the DF-MSE curves were used to determine the temperature for the ^1H DQ-TDNMR experiments, and the temperature was found to be 210°C . This is clearly observed in Figure 2a, which depicts the double-quantum intensities, I_{DQ} , and the reference intensities, I_{REF} , as a function of the experimentally adjusted periods, τ_{DQ} . Details on the ^1H DQ-TDNMR signal acquisition and the meaning of the I_{DQ} vs. τ_{DQ} and I_{REF} vs. τ_{DQ} can be found in Reference [10]. Here, we just state the main features. Both intensities are determined from time-domain NMR signals by applying the pulse sequence described in Reference [17]. This pulse sequence encodes the double-quantum intensities, I_{DQ} , upon the evolution of ^1H nuclear spins in the presence of the so-called ^1H - ^1H magnetic dipolar coupling. On the other hand, ^1H - ^1H dipolar coupling depends on the orientation of the ^1H - ^1H spin pairs in respect to the external magnetic field, and the average of this interaction become zero in the presence of fast isotropic mobile segments. This means that isotropic mobile segments do not generate double quantum coherences, so they do not contribute to I_{DQ} , which can only build up from segments that present any kind of mobility restriction. Thus, in a polymer melt, the I_{DQ} would be directly related to the presence of mobility restrictions associated either with chain entanglements or crosslinks. Moreover, the build-up rate of I_{DQ} with τ_{DQ} is directly related to the residual dipolar coupling (D_{RES}) between ^1H nuclear spins in segments with mobility restriction. Because D_{RES} is inversely proportional to the cube of distance between the nuclear spins, it becomes proportional to the density of points experiencing mobility restrictions, directly translating to the density of entanglements or crosslinks in the polymer. Thus, the I_{DQ} build-up curve (I_{DQ} vs. τ_{DQ}) comprises an initial slope proportional to the density of entanglements/crosslinks. At a longer τ_{DQ} , the I_{DQ} vs. τ_{DQ} curve decays due to transverse relaxation (T_2), so the initial build-up is followed by an exponential-like decay, as observed in the curves shown in Figure 2a. In addition to that, the I_{REF} intensity arises from all molecular segments and only decay due to the T_2 relaxation. An interesting point is that the remaining intensities, I_{REF} , for τ_{DQ} values where I_{DQ} has already decayed will be proportional to segments that do not experience mobility constraints, i.e., free mobile segments. Thus, the long τ_{DQ} tail of the I_{REF} vs. τ_{DQ} curve is only dependent on the free mobile chains.

The I_{DQ} vs. τ_{DQ} and I_{REF} vs. τ_{DQ} curves for PA not exposed and exposed to the H_2S -SCV at 40°C for 15 and 60 days are shown in Figure 2a. They depict the same behavior as reported previously in [10], showing an increasing slope of I_{DQ} vs. τ_{DQ} and a decreasing intensity of the long τ_{DQ} tail I_{REF} vs. τ_{DQ} . This was interpreted as evidence that the H_2S -SCV induced permanent mobility restrictions to the PA chains and reduced the number of free mobile ones. Indeed, an analysis of these functions using proper fitting function based on the motion correlation function lead to the conclusion that these mobility restrictions are likely associated with crosslinks. Therefore, our new set of measurements, for a new batch of PA and other types of ethoxylated H_2S -SCV, reproduce the previously observed behavior very well.

As mentioned, from the analysis based on the motion correlation function, presented in References [10,11], we already know that the H_2S -SCV-induced mobility restrictions are likely to be due to chain crosslinks. Thus, we perform here a different analysis of the I_{DQ} vs. τ_{DQ} and I_{REF} vs. τ_{DQ} curves. This analysis is quite usual in the context of elastomeric networks, where I_{DQ} is intricately linked to crosslinked and/or entangled chains. The first part of the procedure consists on subtracting I_{REF} vs. τ_{DQ} and I_{DQ} vs. τ_{DQ} curves to eliminate the contribution of crosslinked/entangled chains and fitting the extended τ_{DQ} tail of the resulting curve with an exponential function, such as $f_m e^{-\frac{2\tau_{DQ}}{T_{2m}}}$. As mentioned, at a long τ_{DQ} the behavior of I_{REF} vs. τ_{DQ} and, consequently, $(I_{REF} - I_{DQ})$ vs. τ_{DQ} is only

associated with free mobile segments. Thus, the amplitude, f_m , represents the fraction of these segments in the sample, and T_{2m} is the corresponding transverse relaxation time, which is associated with the degree of molecular mobility of these segments. The next step is to use f_m and T_{2m} to obtain the so-called normalized double-quantum intensity, I_{nDQ} , which only depends on the build-up of the double-quantum coherences, i.e., without contribution from the free mobile segments and relaxation [17,18].

$$I_{nDQ}(\tau_{DQ}) = \frac{I_{nDQ}(\tau_{DQ})}{I_{REF}(\tau_{DQ}) + I_{nDQ}(\tau_{DQ}) - f_m e^{-\frac{2\tau_{DQ}}{T_{2m}}}} \quad (1)$$

While the initial slope of the $I_{nDQ}(\tau_{DQ})$ vs. τ_{DQ} curve highlights the information about the residual dipolar coupling proportional to the density of crosslinked/entangled chains, its shape depends on the distribution of D_{RES} , bringing also information about the distribution of the average crosslink density. A proper mathematical procedure based on the Tikhonov regularization, named FITREG and described in References [18,19], is then used to provide the D_{RES} distribution curve.

Figure 2b shows the $I_{nDQ}(\tau_{DQ})$ vs. τ_{DQ} curves obtained for the PA not exposed and exposed to the H₂S-SCV at 40 °C for 15 and 60 days. The increase in the initial slope upon the exposure time becomes rather evident. Moreover, the shape of the curves is also changed for samples more exposed to the H₂S-SCV, suggesting a significant change in the distribution of crosslinks in the sample. The corresponding D_{RES} distribution curves are shown on Figure 2c. The average $\langle D_{RES} \rangle$ values obtained for these curves are present in the legend, showing a rather significant increase, as expected from the slope change.

The changes in the D_{RES} distributions associated with the exposure of the samples to the H₂S-SCV follow a clear pattern. For the non-exposed sample, the distribution comprises an intense and sharp component that peaks at ~50 Hz and a much less intense component peaking at ~250 Hz. These components are likely to be attributed to entanglement chains in the melt state of even a small portion of the crosslinking present on PA. While this bimodal shape seems to be preserved in the samples exposed to the H₂S-SCV, there is a clear and progressive increase in the contribution of components with high D_{RES} values to the distribution upon the exposure time. This is again in line with some H₂S-SCV families promoting the crosslinking of the chains but adds up information in the sense that it shows that it produces a rather inhomogeneous distribution of such crosslinks. This is consistent with the lack of solubility of the exposed H₂S-SCV samples in meta-cresol, which prevented the measure of the CIV in the samples.

Last, we show the evolution of the fraction of free mobile chains, f_m , and the corresponding T_{2m} upon the exposure time in Figure 2d. An evident decrease in f_m and almost constancy of T_{2m} is observed for increasing exposure time. Indeed, the constancy of T_{2m} is indicative that, at 205 °C, all samples are in similar mobility regimes.

3.2. Changes in the PA Chemical Composition Due to Exposure to the H₂S-SCVs

In the former section, we confirmed and further characterized the microstructure and mobility changes induced by the H₂S-SCV in the investigated set of PA samples. We now focus on the possible changes in their chemical composition. To do so, we use two optical techniques, Fourier-Transform Infrared Spectroscopy (FTIR) and Raman spectroscopy, and ¹³C CPMAS high-resolution NMR. All of them offer a detailed analysis of specific molecular groups, allowing them to draw conclusions that are compatible with and complementary to the ¹H TDNMR results previously described.

Figure 3a shows the FTIR spectrum of the samples not exposed and exposed to the H₂S-SCV for 5, 15, 45, and 60 days. The main bands associated with the samples

were assigned in Reference [22]. The attribution to the bands numbered in Figure 3a is 1-4583 cm^{-1} - $\nu(\text{NH})_b$ + Amide III; 2-4871 cm^{-1} - $\nu(\text{NH})_b$ + Amide II; 3-4969 cm^{-1} - $\nu(\text{NH})_b$ + Amide I; 4-5677 cm^{-1} -2 $\cdot\nu_s(\text{CH}_2)$; 5-5784 cm^{-1} -2 $\cdot\nu_a\delta(\text{CH}_2)$; 6-6256 cm^{-1} -Amide I + II) + Amide B; 7-6368 cm^{-1} - $\nu(\text{NH})_b$ + Amide B; 8-6502 cm^{-1} -2 $\cdot\nu(\text{CH}_2)$. One should acknowledge that some bands could not be conclusively assigned based solely on the expected results for the polyamide structure. This suggests that these unassigned peaks are likely attributable not to PA chains, but to another chemical compound present in its composition. Considering that the samples are commercial formulations, it is somewhat expected that, besides polyamide, they contain a significant percentage of additives, with the most common being a plasticizer. Indeed, for the formulations used for pipeline building, it is expected for about 10% of the sample to be a plasticizer, with N-butyl benzene sulfonamide (BBSA) being the plasticizer most used [23,24].

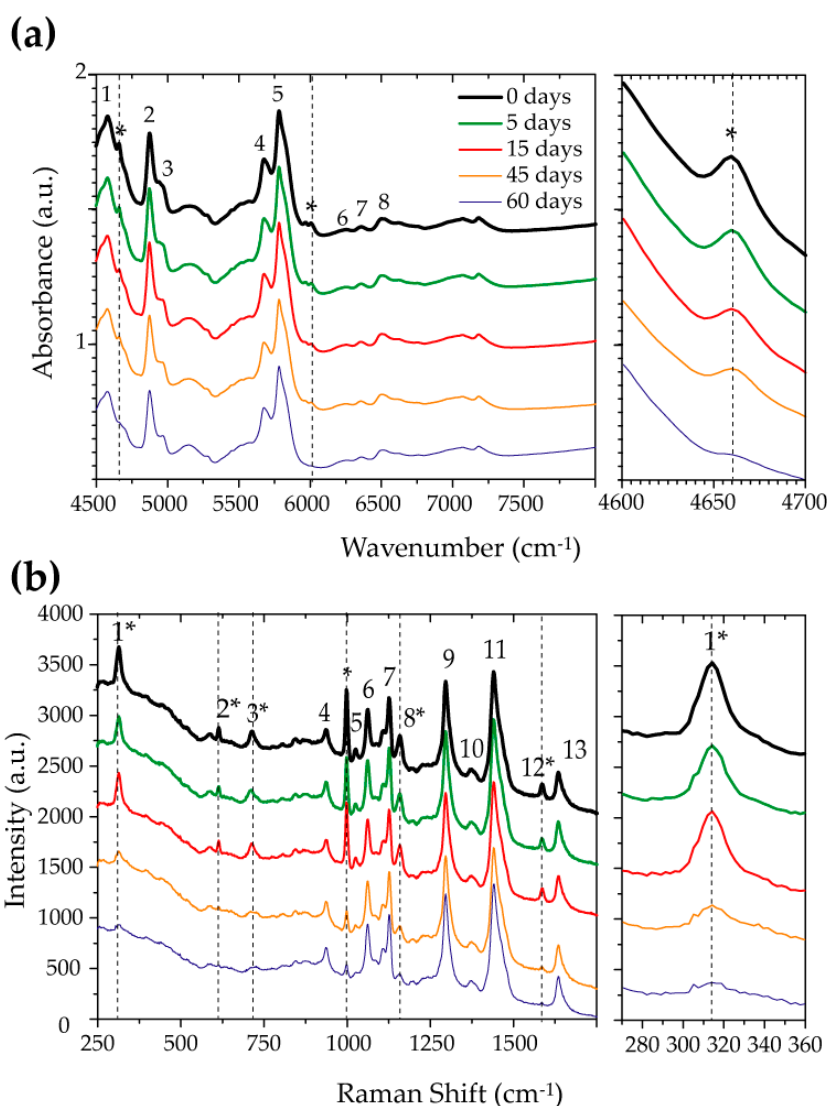


Figure 3. (a) Fourier-Transform Infrared Spectroscopy spectra of PA samples not exposed and exposed for 5, 15, 45, and 60 days. The up numbers correspond to the bands assigned in the text. The bands not attributed to PA are marked with an asterisk. The right panel shows a zoom-in of the 4600 to 4700 cm^{-1} , corresponding to a band not attributed to PA. (b) Raman spectra of PA samples not exposed and exposed for 5, 15, 45, and 60 days. The up-numbers correspond to the bands assigned in the text. The bands not attributed to PA are marked with an asterisk. The right panel shows a zoom-in of 270 to 360 cm^{-1} , corresponding to a band of the BBSA plasticizer.

Figure 3a also shows that the bands associated to the PA structure do not change in the samples exposed to the H₂S-SCV. However, there is a clear decrease in the bands at 4659 cm⁻¹ and 5966 cm⁻¹, as indicated in the figure, with the exposure time. This behavior is highlighted in the lateral panel, which shows a zoom-in of the 4600 cm⁻¹ to 4700 cm⁻¹ spectral regions. This suggests that the chemical structure of the PA is not affected by the exposure to the H₂S-SCV, but there is a progressive removal of additives with the exposure time.

To investigate the specific additive removed from the samples due to the exposure to the H₂S-SCV, we performed Raman spectroscopy measurements, for which the results are shown in Figure 3b. Raman spectra of the PA and the plasticizer BBSA have been already reported in the literature [25]. The main Raman bands shown in Figure 3b are assigned as 1-313 cm⁻¹-C-S stretching-BBSA; 2-612-NH bending-BBSA; 3-715-CH bending-BBSA; 4-936-C=O stretching-polyamide 11; 5-1024-CH bending-BBSA; 6-1064-C-C stretching-polyamide 11; 7-1127-C-C stretching-polyamide 11; 8-1158-CH bending-BBSA; 9-1296-C=N stretching-polyamide 11; 10-1376-CH₂ vibration-polyamide 11; 11-1439-CH₂ vibration-polyamide 11; 12-1585-benzene ring stretching-BBSA; and 13-1635-C=O vibration-polyamide 11.

It can be clearly observed in Figure 3b that six of the identified bands underwent changes with increasing exposure time to the H₂S-SCV. All of these bands, located at wavelengths 313 cm⁻¹, 612 cm⁻¹, 715 cm⁻¹, 1024 cm⁻¹, 1158 cm⁻¹, and 1585 cm⁻¹, are assigned to BBSA. A gradual intensity reduction was observed with prolonged exposure time until a full disappearance in the spectrum of the sample with 60 days of exposure. This is highlighted in the zoomed-in image of the 280 cm⁻¹ to 360 cm⁻¹ regions in Figure 3b. Therefore, the Raman measurements clearly indicate that prolonged exposure to the H₂S-SCV promotes the exudation of the BBSA plasticizer.

Further evidence of the BBSA plasticizer's exudation due to the exposure to the H₂S-SCV was obtained from the ¹³C CPMAS solid-state NMR spectra shown in Figure 4. The spectra of the PA—0 days exhibited in Figure 4a—show all main signals expected for PA (indicated by the green letters), along with some minor signals that can be attributed to the carbons of the BBSA plasticizer (indicated as magenta letters). This was confirmed by comparing the spectra with that of an analytical-grade PA sample (pure PA, not plasticized), also shown in Figure 4a. Those differences in the intensity pattern of the main PA signals can be attributed to differences in the structure of the crystalline phases in each sample [26,27]. However, it is also clear that the signals attributed to the BBSA plasticizer are not present in the spectra of the pure PA sample.

The signals attributed to the BBSA plasticizer are clearly reduced in the ¹³C CPMAS solid-state NMR spectra of the PA—60 days. Besides that, some extra signals also show up in the 60–80 ppm region. This is better observed in Figure 4b, which shows a zoomed-in image of selected spectral regions of the ¹³C CPMAS spectra of PA samples exposed to H₂S-SCV for different time periods. The diminishing of the signals due to the BBSA plasticizer at increasing exposure time is evident from the left and middle panels in Figure 4b, in complete agreement with the results obtained from FTIR and Raman spectroscopies. Moreover, the ¹³C CPMAS spectra of the samples also show the progressive appearance of some signals in the 60–80 ppm region shown in the right panel of Figure 4b. A common characteristic of all H₂S-SCVs used in the O&G industry is that they may be ethoxylated, which means that there would be signals in the 60–80 ppm region. Thus, the ¹³C CPMAS spectra suggest that some chemical groups associated with the H₂S-SCV are incorporated in the samples. Moreover, ¹H-¹³C cross-polarization excitation provides a type of slow mobility filter in the sense that signals from free isotropic mobile molecules do not show up. Thus, the

appearance of signals from typical H₂S-SCV groups in the ¹³C CPMAS spectra suggests that these groups are somewhat immobilized.

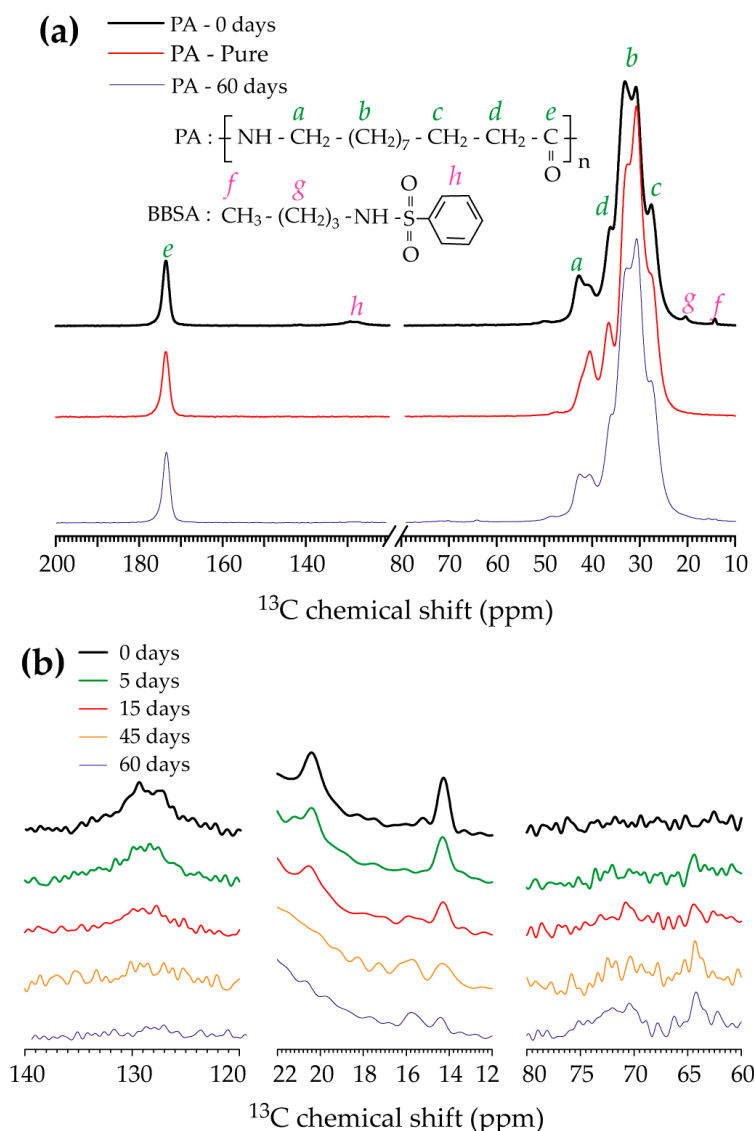


Figure 4. (a) ¹³C CPMAS solid-state NMR spectra of polyamides 11 with the main signals assigned according to the chemical structure of PA and BBSA plasticizer shown as inset. Top, PA—0 days (commercial PA); middle, PA—pure PA, without additives; bottom, PA—60 days (commercial PA exposed to H₂S-SCV for 60 days). (b) Selected spectral regions of the ¹³C CPMAS spectra of PA exposed to H₂S-SCV for the time periods indicated.

4. Discussions

After establishing the primary changes in chemical composition, microstructure, and chain mobility induced by the exposure of PA to H₂S-SCVs, it is crucial to explore the interrelationships among these features.

The removal of plasticizers from polyamide due to exposure to fluids, especially in offshore oil and gas environments, has been shown to significantly impact the polymer's properties [28–31]. Studies indicate that fluid contact, particularly at elevated temperatures, accelerates plasticizer exudation from the PA matrix, leading to increased stiffness, and embrittlement [32]. For example, exposure to oilfield water and chemical additives can promote plasticizer loss, which in turn raises the glass transition temperature (T_g) and reduces chain mobility, adversely affecting mechanical performance [32].

The removal of the BBSA plasticizer in the studied samples was confirmed through FTIR, Raman, and ^{13}C solid-state NMR spectroscopy. Plasticizer additives typically serve to facilitate processing by filling spaces between polymer chains, reducing their interaction, and consequently increasing their mobility [23]. Thus, the elimination of the BBSA plasticizer due to the exposure of PA to the H_2S -SCV appears to be directly associated with the observed increase in the glass transition temperature in the DF-MSE experiments, as shown in Figure 1b and Reference [10]. Additionally, since the plasticizer is a small molecule not chemically bound to PA, it should behave as free mobile segments at temperatures above the melting temperature of PA. Thus, the decrease in the fraction of free mobile segments observed in the ^1H DQ-TDNMR results shown in Figure 2 points to the same direction. It is worth mentioning that thermal and viscometric analysis probes bulk phenomena with no molecular resolution, while optical spectroscopy gives atomic-level information, but mostly associated with the sample's surface due to the reduced penetration depth of the light (for transmission/absorption measurements the thickness of the samples must be reduced). On the other hand, ^{13}C ssNMR spectroscopy probes the sample bulk with atomic resolution, which can be complementary to optical spectroscopy, and time-domain NMR provides specific dynamics information that can be correlated with the thermal measurements. Thus, the NMR measurements suggest that the plasticizer exudation is not restricted to the sample surface and imply motional hindrance of the PA chain motions that may lead to changes in the thermomechanical properties. A more specific analysis on the influence of microstructural change on the mechanical properties is needed.

Thus, our results indicate that the exposure to ethoxylated H_2S -SCVs can promote the exudation of the PA plasticizer even at a low temperature (40°C), which is in line with Reference [32], indicating that it can lead to the same kind of changes in the mechanical properties of the PA samples. Because in offshore oil and gas environments, multiple types of fluids are used, the uses of H_2S -SCVs' cocktails will add up a source that promotes the exudation of the PA plasticizer.

The ^1H DQ-TDNMR experiments demonstrated the increase in the density of dynamically hindered segments in the melt state of PA exposed to the H_2S -SCVs. Thus, the presence of rigidified segments of the H_2S -SCVs, observed by ^{13}C CPMAS, adds another piece of evidence that this dynamic restriction is related to chemical crosslinks induced by the H_2S -SCVs, suggesting that the H_2S -SCV itself may act as a crosslinking agent.

It is known that long-term exposure of polyamide 11 (PA11) to different fluids in extreme environmental conditions can induce significant chemical degradation, primarily through chain scission or crosslinking. Chain scission results in a decrease in molecular weight and intrinsic viscosity, directly compromising mechanical strength and ductility. Mazan and co-workers demonstrated that a reduction in intrinsic viscosity correlates with diminished mechanical properties in degraded PA11 samples [29]. Other studies explored the embrittlement processes in polyamide 11 (PA11) during thermal oxidation. It was suggested that while chain scission is a primary degradation mechanism, crosslinking can also occur, leading to increased brittleness. This study emphasizes that embrittlement is influenced by both molecular weight reduction and changes in crystalline morphology, particularly the interlamellar distance [33,34]. This suggests that inhomogeneous crosslinking contributes to the material's embrittlement over time.

In the ^1H DQ-TDNMR results presented here, there is also evidence of an increase in the crosslink inhomogeneity with the exposure time of the PA to the H_2S -SCV, which can impact the mechanical properties of PA. This is evidence of the lack of solubility of the PA exposed to the H_2S -SCV in meta-cresol.

Finally, the removal of the plasticizer allows PA chains to come into closer proximity, favoring crosslinking reactions involving the H_2S -SCV. This provides an explanation

that links the removal of the plasticizer and the increase in crosslinks suggested by our experimental results.

5. Conclusions

This study investigates the molecular and microstructural transformations of commercial polyamide (PA), used as a barrier layer in flexible pipelines for offshore oil and gas production, when exposed to an ethoxylated H₂S scavenger. A multi-technique analytical approach—comprising FTIR, Raman, ¹³C solid-state NMR, and ¹H time-domain NMR—was employed.

A key finding was the exudation of the BBSA plasticizer, confirmed by FTIR, Raman, and ¹³C solid-state NMR. This plasticizer loss led to a shift in the glass transition temperature due to reduced molecular mobility, as evidenced by Dipolar-Filtered Magic Sandwich Echo (DF-MSE) time-domain NMR, and a decrease in the fraction of highly mobile segments in the melt state, as observed by ¹H Double-Quantum (DQ) time-domain NMR—both performed at low magnetic field. These findings are consistent with previous thermal and viscometric measurements and indicate that plasticizer loss is not restricted to the surface but extends throughout the bulk of the material.

The presence of immobilized segments and reduced solubility in meta-cresol further supports the formation of rigid, crosslinked domains, suggesting that the H₂S-SCV not only promotes plasticizer exudation but may also act as a crosslinking agent. Moreover, ¹H DQ TDNMR revealed increasing inhomogeneity in the crosslinked network with prolonged exposure. The combined effects of plasticizer removal and crosslink formation likely contribute to the degradation of PA's mechanical performance, including embrittlement and reduced ductility.

Overall, the results highlight the need to consider the complex interplay between chemical composition, microstructure, and chain dynamics when evaluating the long-term performance of PA-based barriers in environments containing H₂S-SCVs.

Author Contributions: Conceptualization, A.H.M.d.F.T.d.S., É.G.C. and S.M.C.d.M.; methodology, M.P.d.L., R.H.d.S.G., S.C.d.S.T., L.A.d.O.N., H.d.A.H., S.M.C.d.M., A.P.L., L.S.C.J. and E.R.d.A.; formal analysis, M.P.d.L., A.H.M.d.F.T.d.S., R.H.d.S.G., S.C.d.S.T., É.G.C., L.A.d.O.N., H.d.A.H., S.M.C.d.M., A.P.L., L.S.C.J. and E.R.d.A.; investigation, M.P.d.L., R.H.d.S.G. and J.E.d.O.; writing—original draft, E.R.d.A.; writing—review and editing, M.P.d.L., A.H.M.d.F.T.d.S., R.H.d.S.G., S.C.d.S.T., É.G.C., L.A.d.O.N., H.d.A.H., S.M.C.d.M., A.P.L. and L.S.C.J.; supervision, H.d.A.H. and E.R.d.A.; project administration, A.H.M.d.F.T.d.S., H.d.A.H. and E.R.d.A.; funding acquisition, A.H.M.d.F.T.d.S., H.d.A.H. and E.R.d.A. All authors have read and agreed to the published version of the manuscript.

Funding: This research was funded by Petróleo Brasileiro S.A. (PETROBRAS) through the Cooperation Project 0050.0119730.21.9 and The APC was funded by Conselho Nacional de Desenvolvimento Científico e Tecnológico (CNPq) Grant Number 308760/2022-0.

Institutional Review Board Statement: Not applicable.

Data Availability Statement: Data is available by direct contact with the corresponding author.

Acknowledgments: This research was funded by the Petróleo Brasileiro S.A. (PETROBRAS) through the Cooperation Project 0050.0119730.21.9. ERdA thanks Brazilian agencies FAPESP grants 2017/24465-3 and 2009/18354-8 and CNPq Grant 308760/2022-0.

Conflicts of Interest: Author Antonio Henrique Monteiro da Fonseca Thomé da Silva, Syl-via Correa dos Santos Teixeira, Érica Gervasoni Chaves, Hercílio de Angeli Honorato, Aline Pinde Lima, and Luiz Silvino Chinelatto Junior were employed by the company PETROBRAS. The remaining authors declare that the research was conducted in the absence of any commercial or financial relationships that could be construed as potential conflicts of interest.

References

- Colucci, R.; Frulani, H.; Barbosa, P.; Günther, F.; Cavassin, P.; Couto Faria, G. Recent advances in modeling organic electrochemical transistors. *Flex. Print. Electron.* **2020**, *5*, 13001. [\[CrossRef\]](#)
- Kraft, A.; Grimsdale, A.C.; Holmes, A.B. Electroluminescent Conjugated Polymers—Seeing Polymers in a New Light. *Angew. Chem.-Int. Ed.* **1998**, *37*, 402–428. [\[CrossRef\]](#)
- Lukassen, T.V.; Gunnarsson, E.; Krenk, S.; Glejbøl, K.; Lyckegaard, A.; Berggreen, C. Tension-bending analysis of flexible pipe by a repeated unit cell finite element model. *Mar. Struct.* **2019**, *64*, 401–420. [\[CrossRef\]](#)
- Roseman, M.; Martin, R.; Morgan, G. *Marine Applications of Advanced Fibre-Reinforced Composites*; Elsevier Inc.: Amsterdam, The Netherlands, 2016; pp. 233–257.
- Romão, W.; Castro, E.V.R.; Filho, E.A.S.; Guimarães, R.C.L.; Silva, A.L.N.; Teixeira, S.C.S.; De Paoli, M.A.; De Sena, G.L. Ageing of polyamide 11 used in the manufacture of flexible piping. *J. Appl. Polym. Sci.* **2009**, *114*, 1777–1783. [\[CrossRef\]](#)
- Khalid, H.U.; Ismail, M.C.; Nosbi, N. Permeation Damage of Polymer Liner in Oil and Gas Pipelines: A Review. *Polymers* **2020**, *12*, 2307. [\[CrossRef\]](#)
- Perez-Pineiro, R.; Cruz-Perez, D.; Hoshowski, J.; Zhang, H.; Hendry, J. H₂S Scavenger Tower Operational Efficiency Achieved Through Onsite Compositional Analysis. In Proceedings of the NACE—International Corrosion Conference Series 2018, Phoenix, AZ, USA, 15–19 April 2018.
- Benhabib, M.; Kleinman, S.L.; Peterman, M.C. Quantitative Analysis of Triazine-Based H₂S Scavengers via Raman Spectroscopy. *Ind. Eng. Chem. Res.* **2021**, *60*, 15936–15941. [\[CrossRef\]](#)
- Portela, N.A.; Silva, S.R.C.; de Jesus, L.F.R.; Dalmascio, G.P.; Sad, C.M.S.; Castro, E.V.R.; Morigaki, M.K.; Silva Filho, E.A.; Filgueiras, P.R. Spectroscopic evaluation of commercial H₂S scavengers. *Fuel* **2018**, *216*, 681–685. [\[CrossRef\]](#)
- Perez, M.G.; Lima, A.P.; Moraes, T.B.; Chaves, E.G.; Ruiz, N.M.d.S.; dos Santos Teixeira, S.C.; Honorato, H.d.A.; de Menezes, S.M.C.; deAzevedo, E.R. ¹H Time Domain NMR to probe microstructural and mobility changes in Polyamide 11 exposed to H₂S scavengers. What type of information can be assessed? *Polym. Degrad. Stab.* **2022**, *202*, 110001. [\[CrossRef\]](#)
- Mordvinkin, A.; Saalwächter, K. Microscopic observation of the segmental orientation autocorrelation function for entangled and constrained polymer chains. *J. Chem. Phys.* **2017**, *146*, 094902. [\[CrossRef\]](#)
- Domingos, E.; Pereira, T.M.C.; De Castro, E.V.R.; Romão, W.; De Sena, G.L.; Guimarães, R.C.L. Monitorando a Degradação da Poliamida 11 (PA-11) via Espectroscopia na região do Infravermelho médio com Transformada de Fourier (FTIR). *Polímeros* **2013**, *23*, 37–41. [\[CrossRef\]](#)
- Deshoules, Q.; Le Gall, M.; Dreanno, C.; Arhant, M.; Priour, D.; Le Gac, P.Y. Chemical coupling between oxidation and hydrolysis in polyamide 6—A key aspect in the understanding of microplastic formation. *Polym. Degrad. Stab.* **2022**, *197*, 109851. [\[CrossRef\]](#)
- Brette, M.M.; Holm, A.H.; Drozdov, A.D.; Christiansen, J.d.C. Pure Hydrolysis of Polyamides: A Comparative Study. *Chemistry* **2024**, *6*, 13–50. [\[CrossRef\]](#)
- Filgueiras, J.G.; Cobo, M.F.; Faria, G.C.; Moraes, T.B.; De Azevedo, E.R. *NMR Methods for Characterization of Synthetic and Natural Polymers*, 1st ed.; Zhang, R., Toshikazu, M., Sun, P., Eds.; Royal Society of Chemistry: Cambridge, UK, 2019; Volume 1, pp. 271–298. [\[CrossRef\]](#)
- Filgueiras, J.G.; da Silva, U.B.; Paro, G.; d'Eurydice, M.N.; Cobo, M.F.; deAzevedo, E.R. Dipolar filtered magic-sandwich-echoes as a tool for probing molecular motions using time domain NMR. *J. Magn. Reson.* **2017**, *285*, 47–54. [\[CrossRef\]](#)
- Saalwächter, K. Proton multiple-quantum NMR for the study of chain dynamics and structural constraints in polymeric soft materials. *Prog. Nucl. Magn. Reson. Spectrosc.* **2007**, *51*, 1–35. [\[CrossRef\]](#)
- Chassé, W.; Lang, M.; Sommer, J.U.; Saalwächter, K. Cross-link density estimation of PDMS networks with precise consideration of networks defects. *Macromolecules* **2012**, *45*, 899–912. [\[CrossRef\]](#)
- Saalwächter, K.; Ziegler, P.; Spyckerelle, O.; Haidar, B.; Vidal, A.; Sommer, J.U. H 1 multiple-quantum nuclear magnetic resonance investigations of molecular order distributions in poly (dimethylsiloxane) networks: Evidence for a linear mixing law in bimodal systems. *J. Chem. Phys.* **2003**, *119*, 3468–3482. [\[CrossRef\]](#)
- Papon, A.; Montes, H.; Hanafi, M.; Lequeux, F.; Guy, L.; Saalwächter, K. Glass-transition temperature gradient in nanocomposites: Evidence from nuclear magnetic resonance and differential scanning calorimetry. *Phys. Rev. Lett.* **2012**, *108*, 065702. [\[CrossRef\]](#) [\[PubMed\]](#)
- Baum, J.; Munowitz, M.; Garroway, A.N.; Pines, A. Multiple-quantum dynamics in solid state NMR. *J. Chem. Phys.* **1985**, *83*, 2015–2025. [\[CrossRef\]](#)
- Wu, P.; Siesler, H.W. The assignment of overtone and combination bands in the near infrared spectrum of polyamide 11. *J. Near Infrared Spectrosc.* **1999**, *7*, 65–76. [\[CrossRef\]](#)
- Wypych, G. *Handbook of Plasticizers*, 4th ed.; Elsevier: Amsterdam, The Netherlands, 2023.
- Serpe, G.; Chaupart, N. Relaxation–structure relationship in bulk and plasticized polyamide 11. *J. Polym. Sci. B Polym. Phys.* **1996**, *34*, 2351–2365. [\[CrossRef\]](#)

25. Behler, K.; Havel, M.; Gogotsi, Y. New solvent for polyamides and its application to the electrospinning of polyamides 11 and 12. *Polymer* **2007**, *48*, 6617–6621. [[CrossRef](#)]
26. Hsin, H.Y. Crystal phase transformations in nylon 11. *Mater. Chem. Phys.* **1998**, *56*, 289–293.
27. Johnson, C.G.; Mathias, L.J. Solid-state NMR characterization of copolymers of nylon 11 and nylon 12. *Solid. State Nucl. Magn. Reson.* **1997**, *8*, 161–171. [[CrossRef](#)]
28. Mota, G.P.; da Silva, A.H.M.; da, F.T.; da Rocha, E.B.D.; da Silva, A.L.N. Evaluation of aging process of PA11 from offshore flexible pipe pressure barrier. *Appl. Ocean Res.* **2024**, *144*, 103917. [[CrossRef](#)]
29. Mazan, T.; Jørgensen, J.K.; Echtermeyer, A. Aging of polyamide 11. Part 3: Multiscale model predicting the mechanical properties after hydrolytic degradation. *J. Appl. Polym. Sci.* **2015**, *132*, 42792. [[CrossRef](#)]
30. Celina, M.C. *Polymer Degradation and Stability 2013*; Elsevier: Amsterdam, The Netherlands, 2013; Volume 98, pp. 2419–2429.
31. Dias, F.G.A.; Veiga, A.G.; Gomes, A.P.A.C.P.; Rocco, M.L.M.; da Costa, M.F. The chemical impact of oil fluids in the morphology and thermal properties of the polyamide 11 used in flexible lines. *Discov. Mech. Eng.* **2024**, *3*, 3–13. [[CrossRef](#)]
32. Mazan, T.; Berggren, R.; Jørgensen, J.K.; Echtermeyer, A.J. Aging of polyamide 11. Part 1: Evaluating degradation by thermal, mechanical, and viscometric analysis. *Appl. Polym. Sci.* **2015**, *132*, 6249–6260. [[CrossRef](#)]
33. Okamba-Diogo, O.; Richaud, E.; Verdu, J.; Fernagut, F.; Guilment, J.; Fayolle, B. Investigation of polyamide 11 embrittlement during oxidative degradation. *Polymer* **2016**, *82*, 49–56. [[CrossRef](#)]
34. Okamba-Diogo, O.; Richaud, E.; Verdu, J.; Fernagut, F.; Guilment, J.; Fayolle, B. Molecular and macromolecular structure changes in polyamide 11 during thermal oxidation–Kinetic modeling. *Polym. Degrad. Stab.* **2014**, *108*, 123–132. [[CrossRef](#)]

Disclaimer/Publisher’s Note: The statements, opinions and data contained in all publications are solely those of the individual author(s) and contributor(s) and not of MDPI and/or the editor(s). MDPI and/or the editor(s) disclaim responsibility for any injury to people or property resulting from any ideas, methods, instructions or products referred to in the content.